Bulletin of Geology
e-ISSN 2580-0752
e-ISSN 2580 – 0752
Fakultas Ilmu dan Teknologi Kebumian
Institut Teknologi Bandung
www.buletingeologi.com

NUMERICAL SIMULATION OF TSUNAMI GENERATED BY THE DENSE PYROCLASTIC DEPOSIT LANDSLIDE FROM THE 1815 TAMBORA CALDERA ERUPTION

RIYADI ZAKIA SYAHRULLOH[1*], HAMZAH LATIEF[1,2], KARINA APRILIA SUJATMIKO[1,2], DAN IDHAM ANDRI KURNIAWAN[3]

1. Earth Sciences Study Program, Faculty of Earth Sciences and Technology, Institut Teknologi Bandung (ITB), Jl. Ganesa No. 10, Bandung, West Java, Indonesia
2. Coastal and Marine Resources Development Center (PPWPL), Institut Teknologi Bandung (ITB), Labtek VI, 4th Floor, Jl. Ganesa No. 10, Bandung, West Java, Indonesia
3. Geological Engineering Study Program, Faculty of Earth Sciences and Technology, Institut Teknologi Bandung (ITB), Jl. Ganesa No. 10, Bandung, West Java, Indonesia

*Email: riyadizakia111@gmail.com

Abstract – The 1815 eruption of the Tambora caldera was one of the most powerful volcanic events ever recorded and generated tsunamis that affected coastal areas around Sumbawa and parts of East Java. One mechanism thought to have contributed to tsunami generation is the entry of dense pyroclastic flow deposits into the sea. This study conducts numerical simulations using COMCOT version 1.7 Beta and TUNAMI N1 to model tsunami waves produced by two potential triggering mechanisms: dense pyroclastic deposit landslides and artificial waves representing non-landslide processes. The simulations were applied to several potential source zones identified from geological evidence around the caldera. The primary objective of this research is to evaluate and compare the accuracy of these two mechanisms by examining how well each reproduces the historical characteristics of the 1815 tsunami, particularly wave heights and arrival times in both near-source and far-field regions. The results show that the artificial-wave scenario produces wave heights that greatly exceed historical accounts in proximal areas, with values of 16.17 meters at Tambora and 14.67 meters at Sanggar. In contrast, the dense-landslide scenario yields 6 meters and 3.67 meters at these locations, values that closely match historical reports of 5 to 6 meters and 4 meters. In distal regions such as Sumenep and Besuki, both scenarios underestimate the recorded tsunami heights, producing less than 1 meter compared with documented values of 1 to 2 meters. These discrepancies suggest the presence of additional tsunami-generating processes not captured by the models. Overall, the dense-landslide scenario offers a more realistic representation of the near-field tsunami impacts, while further refinement is required to fully account for the observed effects in more distant areas.

Key words: volcanic tsunami, Mount Tambora, solid landslides, artificial waves.

Sari – Letusan kaldera Gunung Tambora pada tahun 1815 merupakan salah satu peristiwa vulkanik terkuat yang pernah tercatat dan memicu tsunami yang berdampak pada wilayah pesisir di sekitar Sumbawa hingga sebagian Jawa Timur. Salah satu mekanisme yang diduga berkontribusi terhadap pembangkitan tsunami tersebut adalah masuknya endapan aliran piroklastik padat ke laut. Penelitian ini melakukan simulasi numerik menggunakan COMCOT versi 1.7 Beta dan TUNAMI N1 untuk memodelkan gelombang tsunami yang dihasilkan oleh dua mekanisme pemicu potensial, yaitu longsoran padat endapan piroklastik dan gelombang buatan yang merepresentasikan proses non-longsoran. Skenario simulasi diterapkan pada beberapa zona sumber potensial yang diidentifikasi berdasarkan bukti geologi di sekitar kaldera. Tujuan utama penelitian ini adalah mengevaluasi dan membandingkan keakuratan kedua mekanisme tersebut dengan menilai sejauh mana masing-masing mampu mereproduksi karakteristik historis tsunami tahun 1815, khususnya tinggi gelombang dan waktu tiba, baik di wilayah dekat sumber maupun jauh dari sumber. Hasil simulasi menunjukkan bahwa skenario gelombang buatan menghasilkan tinggi gelombang yang jauh melampaui catatan historis di wilayah proksimal, yaitu 16,17 meter di Tambora dan 14,67 meter di Sanggar. Sebaliknya, skenario longsoran padat menghasilkan tinggi gelombang 6 meter dan 3,67 meter pada lokasi yang sama, nilai yang lebih mendekati laporan historis setinggi 5 hingga 6 meter dan 4 meter. Di wilayah distal seperti Sumenep dan Besuki, kedua skenario menghasilkan gelombang kurang dari 1 meter, lebih rendah daripada catatan historis 1 hingga 2 meter. Ketidaksesuaian ini mengindikasikan kemungkinan adanya proses pembangkitan tsunami tambahan yang belum terwakili dalam model. Secara keseluruhan, skenario longsoran padat memberikan representasi yang lebih realistis terhadap dampak tsunami di wilayah dekat sumber, sementara pemodelan di wilayah jauh masih memerlukan penyempurnaan untuk sepenuhnya menjelaskan dampak yang tercatat.

Kata kunci: tsunami vulkanik, Gunung Tambora, longsoran padat, gelombang buatan.

1. INTRODUCTION

The 1815 eruption of Mount Tambora stands as one of the most powerful volcanic events in human history, reaching a Volcanic Explosivity Index (VEI) of 7 and releasing an immense volume of pyroclastic material estimated between 30 and more than 300 km³ (Self *et al*., 1984). The eruption caused severe local destruction and triggered global climatic anomalies, while also generating secondary hazards such as landslides and tsunamis across central Indonesia. Contemporary reports describe tsunami impacts along the coasts surrounding Sumbawa Island and extending eastward to Besuki and Sumenep in East Java, indicating that the event had a broad regional influence. A general reconstruction of the 1815 eruption chronology, based on historical accounts and pyroclastic stratigraphy, is shown in **Figure 1**.

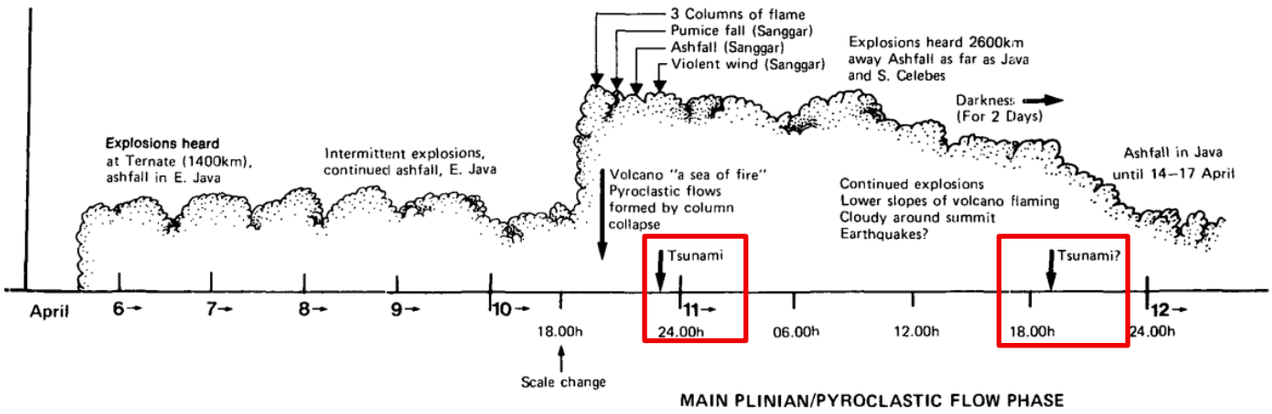

Figure 1. Chronology of the 1815 eruption reconstructed using evidence from contemporary reports combined with pyroclastic stratigraphy (Self *et al*., 1984).

Despite the recognition of tsunami occurrences during the Tambora eruption, the physical mechanism responsible for generating these waves remains uncertain. Several hypotheses have been proposed, including the rapid entry of pyroclastic flows into the sea, partial caldera collapse, and atmospheric pressure disturbances resulting from eruptive blasts. However, numerical studies that explicitly test and compare these mechanisms, particularly through multiple generation scenarios, are still limited. Previous research has demonstrated that dense volcanic landslides were capable of producing significant tsunamis, as shown in studies from Montserrat and Myojin-sho (Pelinovsky *et al*., 2004). Similarly, modeling approaches applied to the 1883 Krakatau eruption (Maeno and Imamura, 2011) have shown that pyroclastic flows entering the sea can be treated as dense masses capable of deforming the water surface. In addition, artificial-wave models based on idealized energy inputs have been used to investigate non-tectonic tsunami sources, such as those described by Watts (1998).

Although these approaches have been successfully applied in several volcanic settings, no study has specifically examined the 1815 Tambora tsunami using a combined modeling framework that includes both dense pyroclastic deposit landslides and artificial-wave initiation. Furthermore, there has been limited effort to evaluate which mechanism more accurately reproduces the historical characteristics of the tsunami, particularly in terms of wave height distribution and arrival times at both near-source and far-field regions.

To address this gap, the present study develops a numerical simulation of the 1815 Tambora tsunami using two generation scenarios: (1) a dense landslide scenario representing the entry of pyroclastic flow deposits into the sea, and (2) an artificial-wave scenario representing non-landslide triggers such as atmospheric pressure disturbances. Historical geological data from Self *et al*. (1984), Sigurdsson and Carey (1989), and Suhendro *et al*. (2021) were integrated to reconstruct pre-eruption topography and to identify the most plausible source zones around the caldera. The primary objective of this study is to evaluate and compare the accuracy of these two tsunami-generation mechanisms by assessing their ability to reproduce historical tsunami characteristics recorded during the 1815 event. This evaluation focuses on simulated wave heights and arrival times in both near-source and far-field regions to determine which mechanism provides a closer representation of the documented tsunami impacts.

2. DATA AND METHODS

2.1 Data

The reconstruction of pre-eruption bathymetry and topography was carried out by combining recent datasets from BATNAS (6 arcsecond resolution) and DEMNAS (0.27 arcsecond resolution) with historical geological information from Self *et al*. (1984), Sigurdsson and Carey (1989), and Suhendro *et al*. (2021). This process involved calculating the difference between the current elevation or depth data and the estimated thickness of eruption deposits obtained from field observations, which average around 20 meters. For instance, if the current bathymetric data indicate a sea depth of 50 meters, the pre-eruption depth is estimated to be 30 meters. Both datasets were then interpolated to reconstruct the pre-eruption topographic and bathymetric conditions based on geological evidence from the aforementioned studies. **Figure 2** and **Figure 3** illustrate the estimated changes in bathymetry and topography before and after the 1815 eruption in the vicinity of Mount Tambora.

2.2 Research Methods

The tsunami simulation in this study was conducted using two primary numerical models: COMCOT version 1.7 Beta (Cornell Multi-grid Coupled Tsunami Model) and TUNAMI N1 (Tohoku University's Numerical Analysis Model for Investigation).

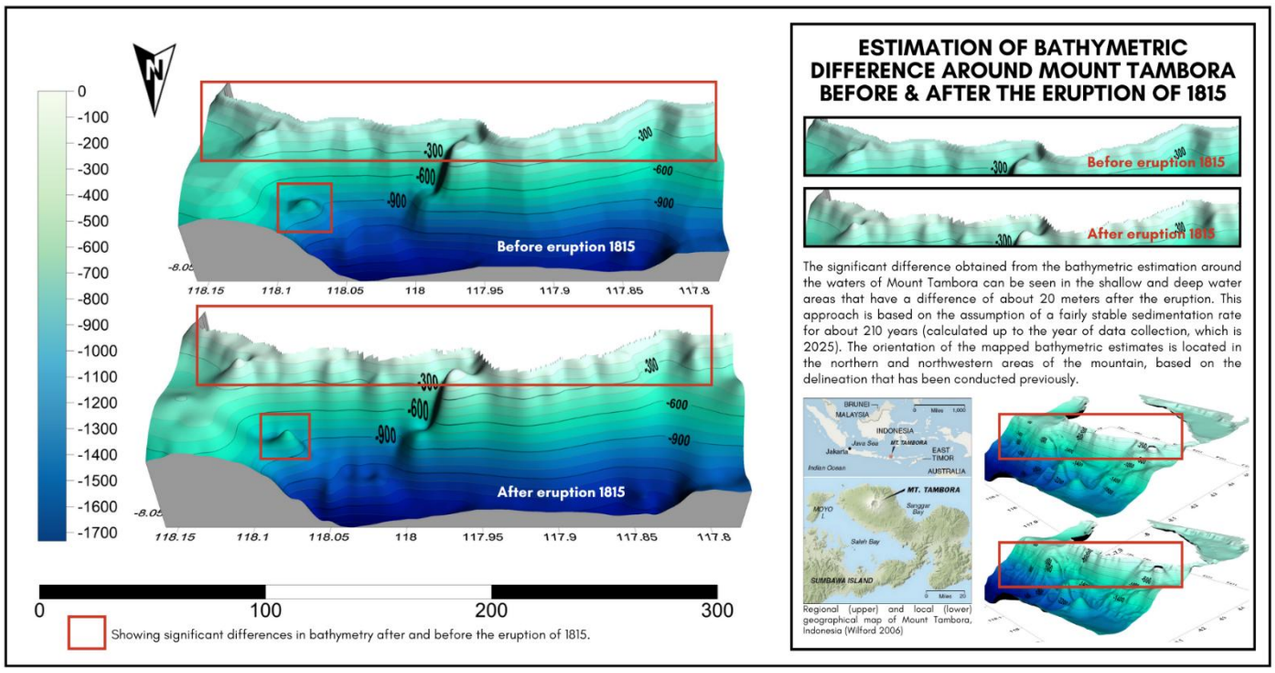

Figure 2. Estimated changes in bathymetry before and after the 1815 eruption

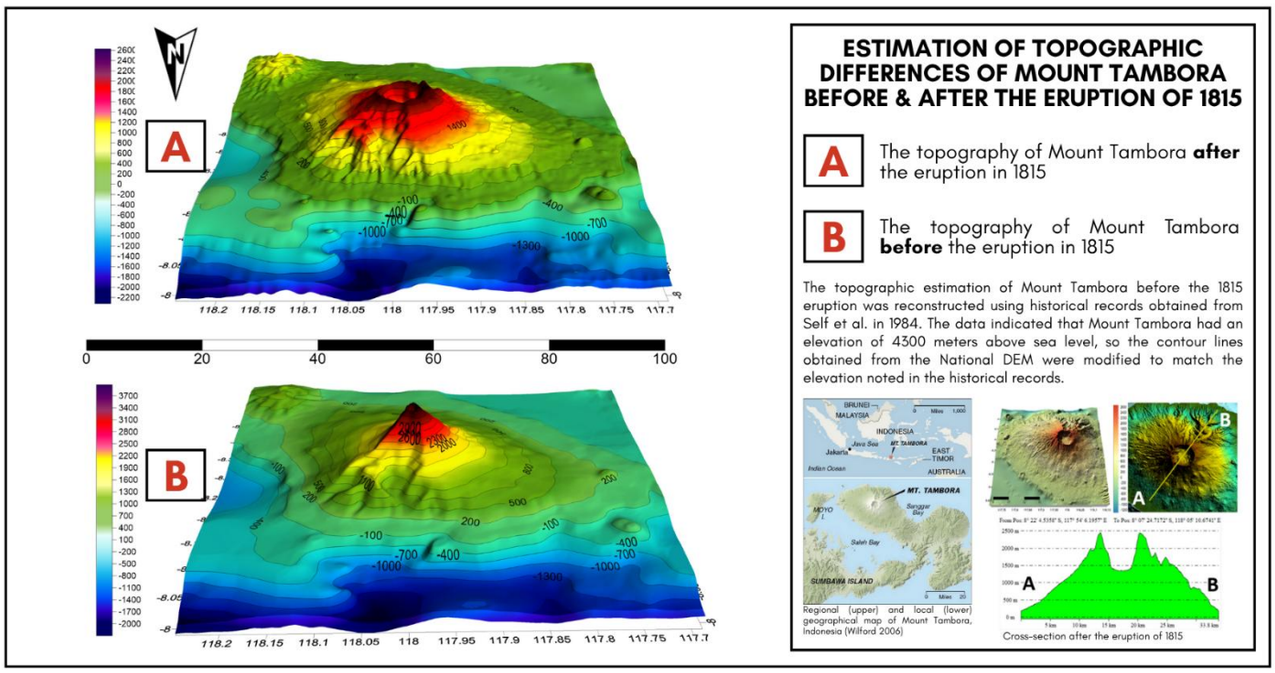

Figure 3. Estimated changes in topography after and before the 1815 eruption

2.2.1 COMCOT Model

The COMCOT model was employed to simulate tsunami generation and propagation caused by a dense landslide originating from the central caldera of Mount Tambora. This landslide represents pyroclastic flows that had lost their gas pressure and transformed into dense masses upon reaching the sea. The landslide parameters were based on an estimated volume of 18 km³ as proposed by Kandlbauer and Sparks (2014), while the landslide trajectory was determined from the distribution of pyroclastic flow deposits described by Sigurdsson and Carey (1989), as shown in **Figure 4**. The landslide mass was assumed to be homogeneous and to move under the influence of gravity, without considering internal dynamics such as temperature and pressure variations.

2.2.2 TUNAMI N1 Model

The TUNAMI N1 model was used to simulate the artificial wave scenario, representing tsunamis generated by non-landslide sources such as explosions or atmospheric pressure waves. The initial wave height was estimated using the semi-empirical formulation by Watts (1998), which incorporates parameters such as the width and height of the landslide and the local sea depth at the source region. **Figure 4** illustrates the conceptual model used to define wave initiation and the spatial distribution of pyroclastic flow deposits produced by the 1815 eruption of Mount Tambora.

Figure 4 illustrates the reconstructed distribution of pyroclastic flow deposits (PFDs) and the potential locations for artificial tsunami wave initiation triggered by dense landslides resulting from the

1815 eruption of Mount Tambora. The white circles represent data from Self *et al*. (1984), the black circles indicate findings from Suhendro *et al*. (2021), and the yellow circles show the locations and data from Sigurdsson and Carey (1989). These three datasets were integrated to combine geological and morphological evidence from post-eruption studies in order to estimate the direction of pyroclastic flow movement and identify potential landslide zones toward the sea.

The main map shows the Tambora caldera along with the estimated trajectory of pyroclastic density currents (PDCs) that lead to several sectors, including Oi Marai, Katupa, Labu Bili, Labu Na'e, Doro Bente, and Sarae Nduha, which are considered the starting points for potential tsunami generation. The color scale shows the change in elevation from 0 to more than 25 meters, which describes the initial amplitude of the wave for each location based on a semi-empirical formula from Watts (1998). The integration of the three studies provides a scientific basis for identifying the most likely tsunami source zones associated with the 1815 post-Tambora eruption pyroclastic sediment landslide.

2.2.3 Model Parameters

The simulation was conducted over a 5-hour period following the main eruption of April 10, 1815, at 23:00 local time. The analyzed outputs include the distribution of maximum sea surface height, tsunami arrival time, and wave propagation patterns for each scenario. The simulation results were qualitatively validated by comparing the modeled tsunami wave heights with historical records from several affected areas, including Besuki, Sumenep, Sanggar, Sumbawa, Bima, and the coastal region of Mount Tambora, based on data from Soloviev and Go (1974) and Stothers (1984). **Table 1** refers to the input parameters used on the model.

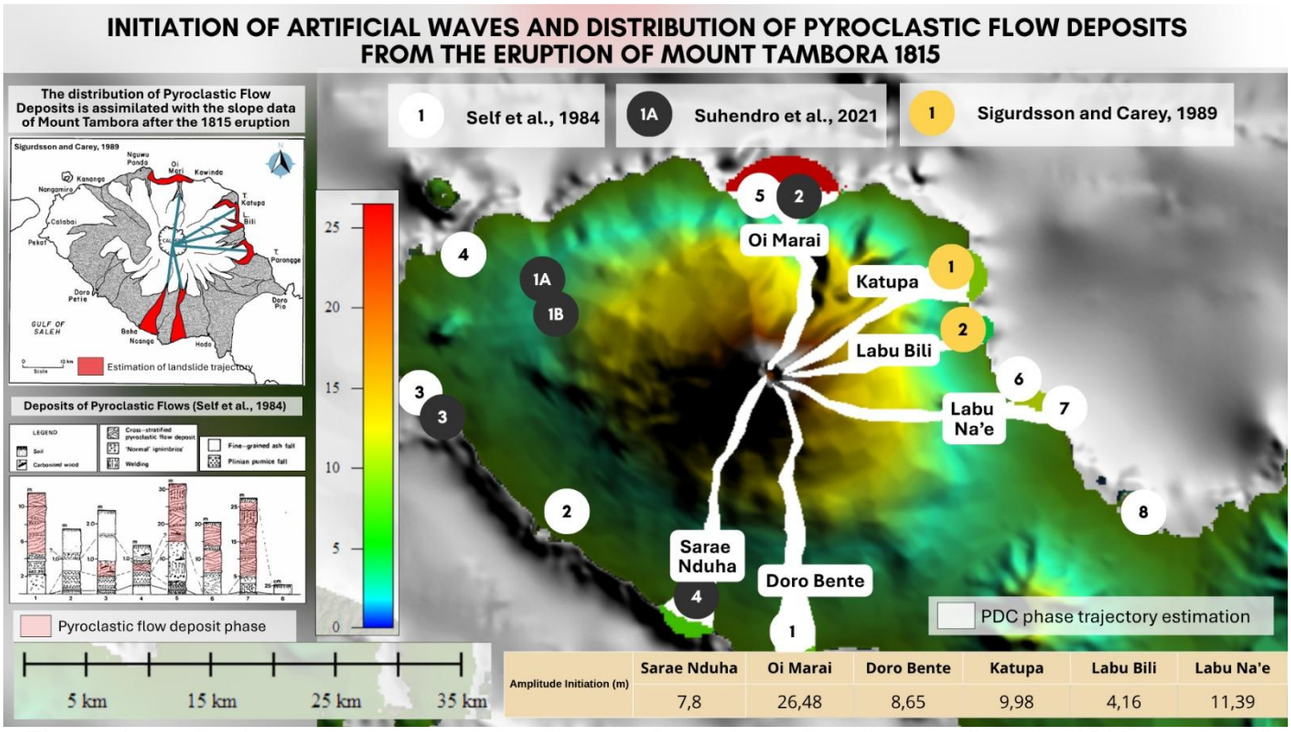

Figure 4. Artificial wave initiation and distribution of pyroclastic flow deposits from the 1815 eruption of Mount Tambora

Tabel 1. Schematic of the Landslide Scenario Parameters

Nama	Length (m)	Width (m)	Thickness (m)	Reference	Slope (°)	Frac (%)
Sarae Nduha	12890	5450	4	Suhendro *et al*., 2021	9.8	74
Oi Marai	11310	11360	12	Suhendro *et al*., 2021	11.34	58
Doro Bente	13680	3639	3	Self *et al*., 1984	8.86	81
Katupa	16050	4540	12	Self *et al*., 1984 Sigurdsson and Carey, 1989	8.78	69
Labu Bili	15260	2270	10	Self *et al*., 1984 Sigurdsson and Carey, 1989	8.49	56
Labu Na'e	12890	4540	18.5	Sigurdsson and Carey, 1989	8.69	65

The standard methods in COMCOT and TUNAMI were applied without modification to their core mathematical structures, as illustrated in **Figure 5**. However, several input and parameter adjustments

were introduced to align the model setup with the historical characteristics of the 1815 Tambora eruption. One key adaptation involved the manual reconstruction of topography and bathymetry based on historical geological data, as well as the separation of two generation scenarios the landslide scenario and the artificial wave scenario to better represent the complex tsunami sources believed to have occurred during the 1815 event.

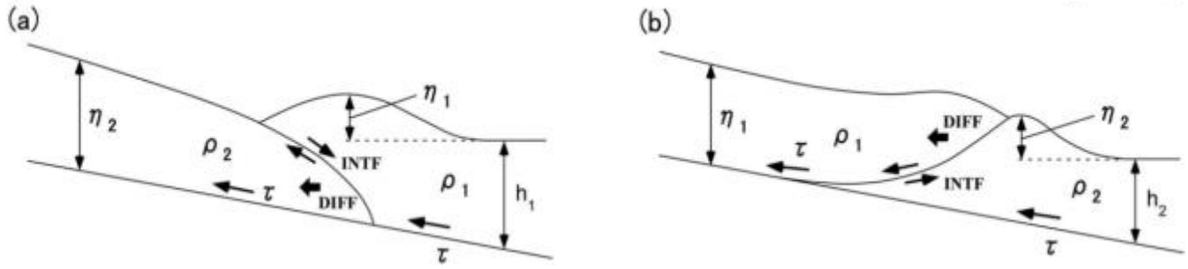

Figure 1. Two types of two-layer shallow water models that depict pyroclastic flows as they enter the sea (a) Solid-type model (b) Light-type model (Maeno and Imamura, 2011)

Upper Layer (Representative of Water)

$$\frac{\partial(\eta_1 - \eta_2)}{\partial t} + \frac{\partial P_1}{\partial x} + \frac{\partial Q_1}{\partial y} = 0 \quad (1)$$

$$\frac{\partial P_1}{\partial t} + \frac{\partial}{\partial x}\left(\frac{P_1^2}{D_1}\right) + \frac{\partial}{\partial y}\left(\frac{P_1 Q_1}{D_1}\right) + gD_1\frac{\partial \eta_1}{\partial x} + \frac{\tau_x}{\rho_1} - INTF_x = 0 \quad (2)$$

$$\frac{\partial Q_1}{\partial t} + \frac{\partial}{\partial y}\left(\frac{Q_1^2}{D_1}\right) + \frac{\partial}{\partial x}\left(\frac{P_1 Q_1}{D_1}\right) + gD_1\frac{\partial \eta_1}{\partial y} + \frac{\tau_y}{\rho_1} - INTF_y = 0 \quad (3)$$

Down Layer (Representative of Landslide)

$$\frac{\partial \eta_2}{\partial t} + \frac{\partial P_2}{\partial x} + \frac{\partial Q_2}{\partial y} = 0 \quad (4)$$

$$\frac{\partial P_2}{\partial t} + \frac{\partial}{\partial x}\left(\frac{P_2^2}{D_2}\right) + \frac{\partial}{\partial y}\left(\frac{P_2 Q_2}{D_2}\right) + gD_2\left(\alpha\frac{\partial D_1}{\partial x} + \frac{\partial \eta_2}{\partial x} - \frac{\partial h_1}{\partial x}\right) + \frac{\tau_x}{\rho_2} - \alpha INTF_x = DIFF_x \quad (5)$$

$$\frac{\partial Q_2}{\partial t} + \frac{\partial}{\partial y}\left(\frac{Q_2^2}{D_2}\right) + \frac{\partial}{\partial x}\left(\frac{P_2 Q_2}{D_2}\right) + gD_2\left(\alpha\frac{\partial D_1}{\partial y} + \frac{\partial \eta_2}{\partial y} - \frac{\partial h_1}{\partial y}\right) + \frac{\tau_y}{\rho_2} - \alpha INTF_y = DIFF_y \quad (6)$$

with :

$$D_1 = \eta + h \quad (7)$$

$$D_2 = \eta_2 \quad (8)$$

$$\frac{\tau_x}{\rho} = \frac{gn_b^2}{D^{\frac{7}{3}}} M\sqrt{M^2 + N^2} \quad (9)$$

$$\frac{\tau_y}{\rho} = \frac{gn_b^2}{D^{\frac{7}{3}}} N\sqrt{M^2 + N^2} \quad (10)$$

$$INTF_x = f\bar{u}\sqrt{\bar{u}^2 + \bar{v}^2} \quad (11)$$

$$INTF_y = f\bar{v}\sqrt{\bar{u}^2 + \bar{v}^2} \quad (12)$$

$$DIFF_x = k\sqrt{\frac{\partial^2 M}{\partial x^2} + \frac{\partial^2 M}{\partial y^2}} \quad (13)$$

$$DIFF_y = k\sqrt{\frac{\partial^2 N}{\partial x^2} + \frac{\partial^2 N}{\partial y^2}} \quad (14)$$

The elevation of the water level is denoted by η_1, while the thickness of the flow is expressed by η_2. The total depth of the waters is indicated by D_1 and the depth of landslide by D_2. The flow velocity in the x and y directions is denoted by P and Q, respectively. Water density is denoted by ρ, while α denotes the ratio between water density and flow. The friction at the base of the surface in the direction of x or y is written as τ. The shear force between surfaces is denoted by INTF, and the turbulent diffusion force by DIFF. The coefficient of interface drag or interfacial drag is expressed by f. The relative velocity between the flow and seawater in the x and y directions is represented by $\bar{u}$ and $\bar{v}$ respectively. Furthermore, the turbulent diffusion coefficient is represented by k, and . It shows the coefficient of basic roughness and, g is the acceleration of gravity used in the calculation of the force and motion of the fluid.

3. RESULTS

3.1 Tsunami Propagation Time

Numerical simulations were carried out using two tsunami generation scenarios, namely a solid landslide originating from the central caldera of Mount Tambora, and an artificial wave represented by an estimated sea level elevation resulting from pyroclastic flow deposits. The simulation results show significant differences in both the maximum height of the tsunami and the time of arrival of the waves at various observation points, as summarized in **Table 2.**

Table 2. Tsunami propagation time based on model simulation results

Region	Landslide Scenario	Artificial Waves Scenario	History
Tambora	4 minutes	0 minutes	-
Sanggar	12 minutes	2 minutes	-
Sumbawa	30 minutes	10 minutes	-
Bima	25 minutes	8 minutes	-
Sumenep	115 minutes	110 minutes	Around 2 Hours after erupted
Besuki	125 minutes	120 minutes	Around 2 Hours after erupted

As shown in **Table 2**, the earliest tsunami arrival times occurred in areas adjacent to the source, especially around Tambora and Sanggar, while more distant areas such as Sumenep and Besuki recorded wave propagation times that exceeded two hours. **Figure 6** shows the spatial distribution of tsunami arrival time for artificial wave scenarios, with a color scale showing the time of propagation of tsunami waves produced by the eruption of Mount Tambora in 1815 in minutes. The wave propagation pattern appears to be radial, but shows directional distortion due to the interaction between the topography of the seabed and the small islands around Sumbawa Island.

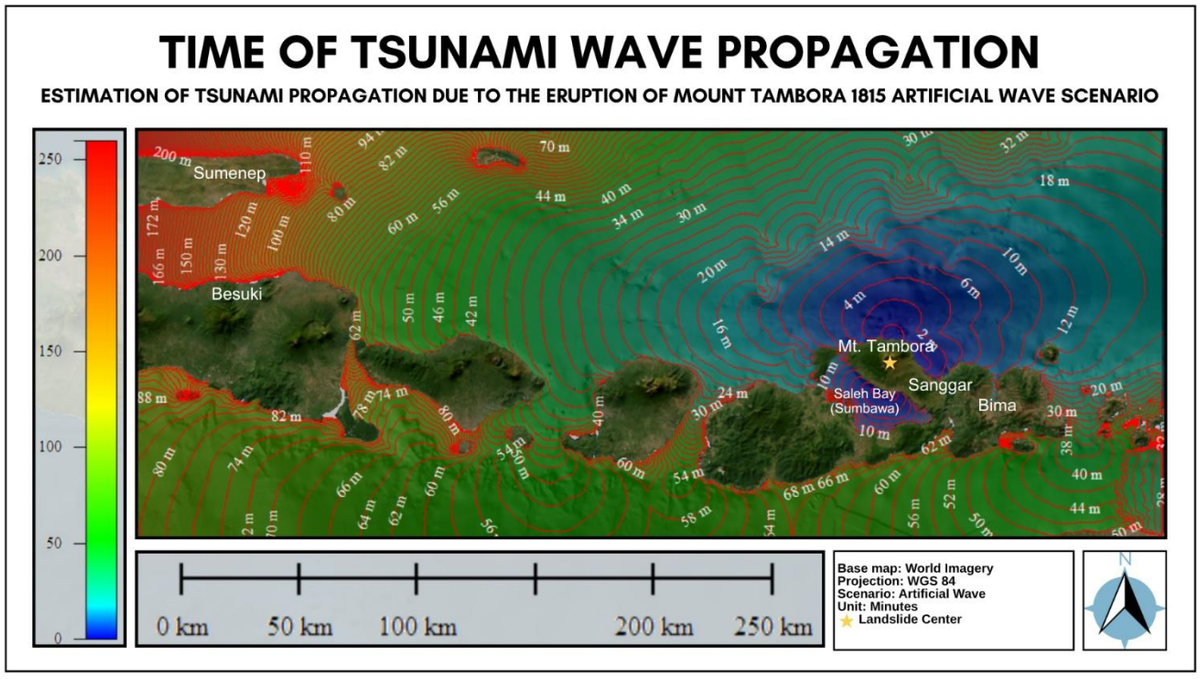

Figure 6. Tsunami propagation time resulting from the eruption of Mount Tambora

3.2 Maximum Tsunami Height and Historical Validation

The maximum sea surface elevations for each simulation scenario are presented in **Figure 7** to **Figure 9**. The landslide scenario produced a tsunami with a maximum height of approximately 6 meters along the Tambora coast, decreasing to about 3.67 meters in Sanggar, and further diminishing at more distant locations. In contrast, the artificial wave scenario generated a maximum tsunami height of 16.17 meters near Tambora and 14.67 meters in Sanggar. This difference is likely due to the higher source energy in the artificial wave scenario, while the landslide-induced tsunami experienced energy loss due to friction along the mountain slope. **Table 3** summarizes the differences in maximum wave heights between the two scenarios.

Table 3. Maximum wave height data at observation points for the artificial wave scenario

Region	Artificial Waves (m)	Landslide Scenario (m)	History
Tambora	16.17	6	5 m - 6 m
Sanggar	14.67	3.67	4 m
Sumbawa	2.39	0.15	0.5 m – 3.5 m
Bima	1.76	0.42	Run- up 0.3 m
Sumenep	0.76	0.33	1 m – 1.5 m
Besuki	0.11	0.09	1 m - 2 m

BULLETIN OF GEOLOGY, VOL. 9 NO. 1,
DOI: 10.5614/bull.geol.2025.9.1.4.

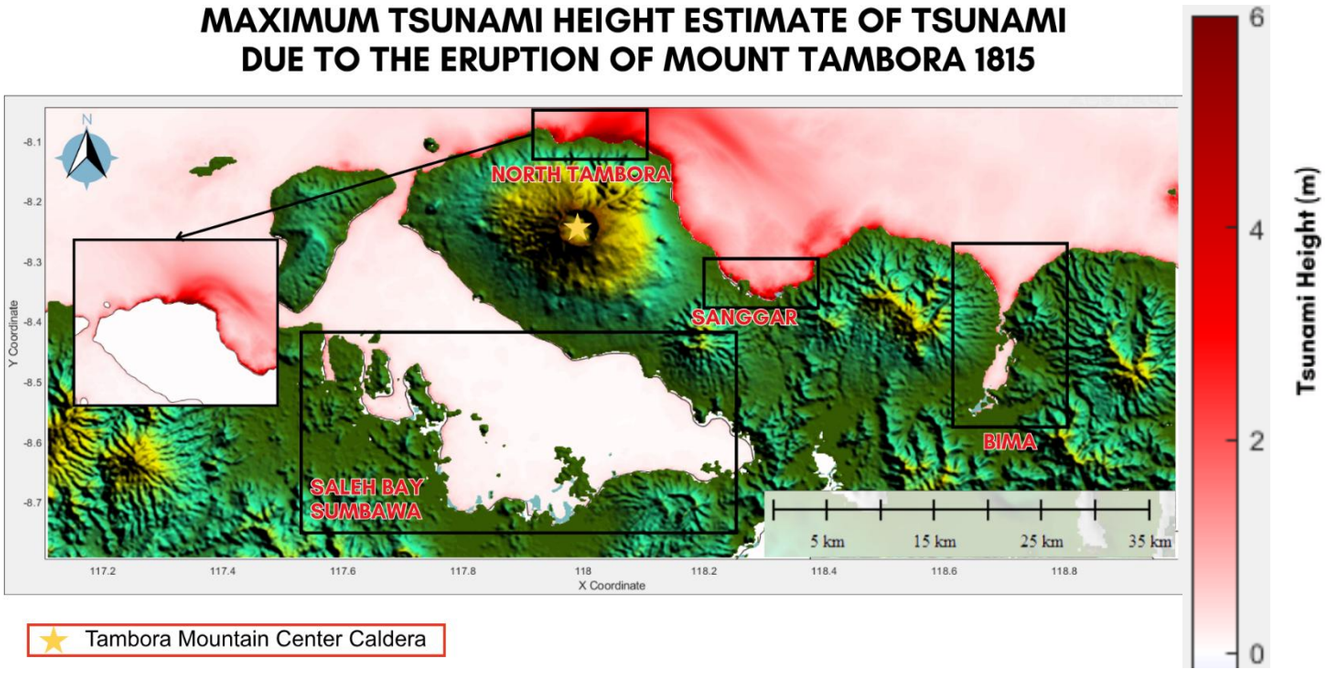

Figure 7. Maximum tsunami height in the Tambora, Sanggar, Bima, and Sumbawa areas for the landslide scenario

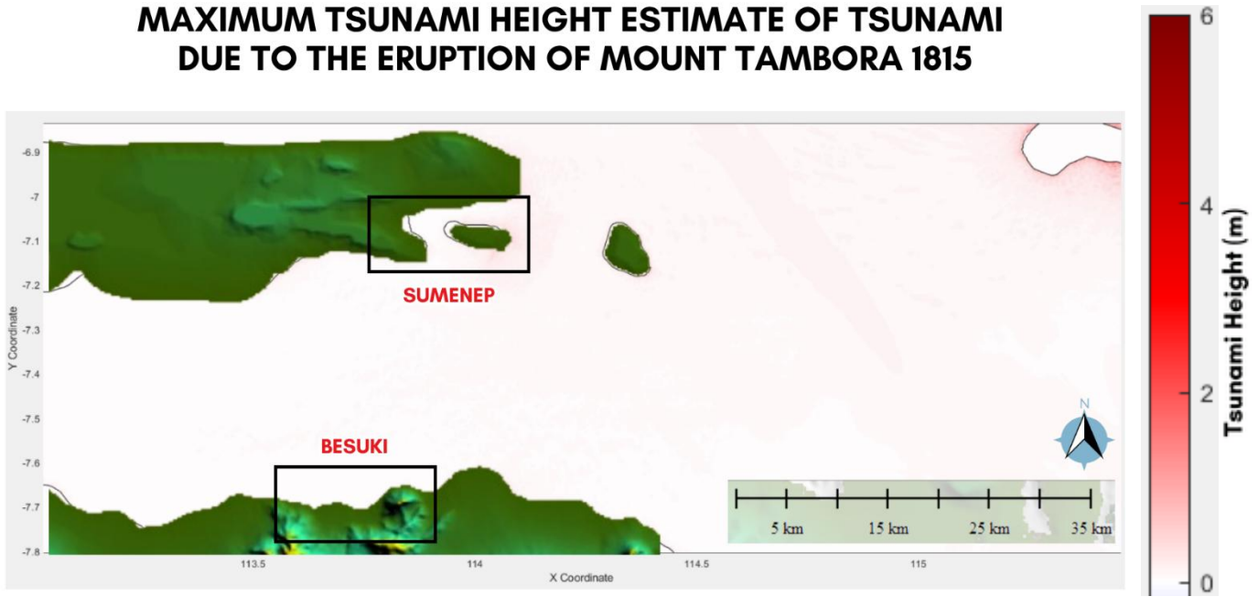

Figure 8. Maximum tsunami height in the Sumenep and Besuki areas for the landslide scenario

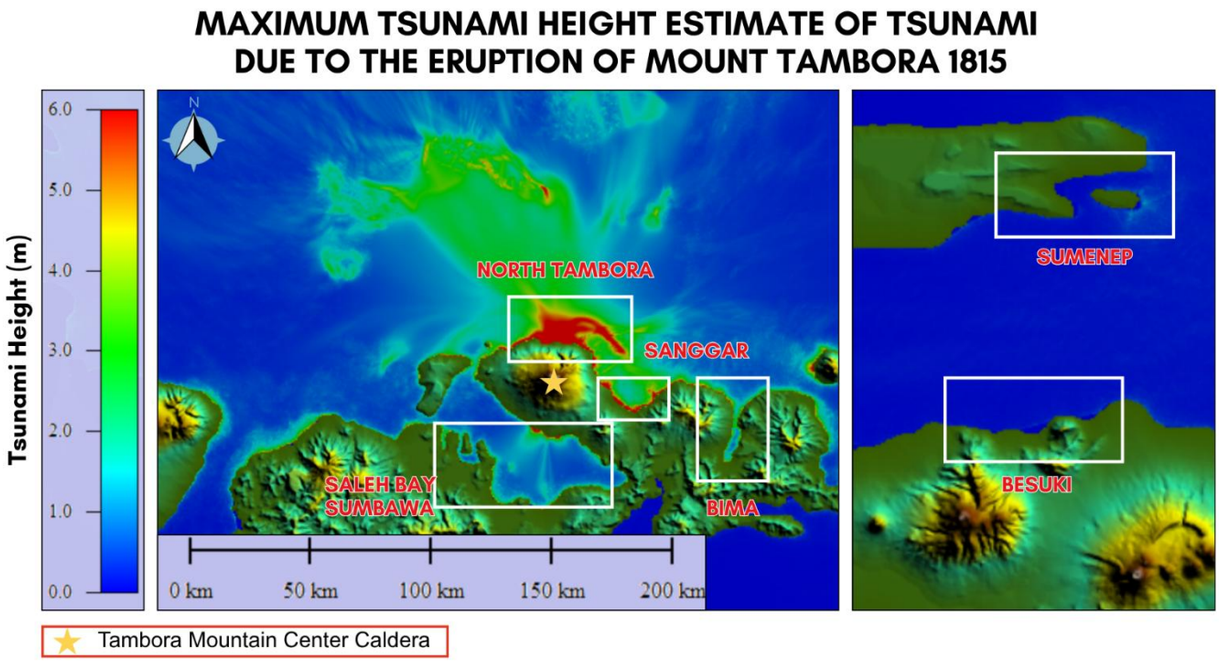

Figure 9. Maximum tsunami height for the artificial wave scenario

BULLETIN OF GEOLOGY, VOL. 9 NO. 1,
DOI: 10.5614/bull.geol.2025.9.1.4.

Validation was carried out by comparing the simulation results with historical records. The tsunami heights simulated for Tambora and Sanggar were consistent with the reports of Soloviev and Go (1974), which recorded wave heights of 5–6 meters at Tambora and 4 meters at Sanggar. However, in more distant regions such as Sumenep and Besuki, the simulation produced maximum wave heights of only 0.33 meters and 0.09 meters, respectively lower than the historical accounts reporting 1–2 meters. This discrepancy suggests the possible involvement of additional tsunami sources, such as atmospheric pressure waves or a secondary eruptive phase (Self *et al*., 1984).

4. DISCUSSION

4.1 Comparison of Tsunami Heights with Historical Records

The simulation results show that the artificial wave scenario generated higher wave amplitudes than the dense landslide scenario. This is because artificial waves do not experience energy dissipation from frictional interactions with the ground surface, unlike the landslide-induced tsunami, which lost significant energy during downslope movement.

The spatial distribution of tsunami heights at Tambora, Sanggar, and Bima showed a strong agreement with historical records. The model produced maximum heights of 6 m (Tambora), 3.67 m (Sanggar), and 0.42 m (Bima), closely matching the observed values of 5–6 m, 4 m, and run up 0.3 m, respectively (Soloviev and Go, 1974; Stothers, 1984). In contrast, the results for Sumenep (0.33 m) and Besuki (0.09 m) were lower than the recorded 1–1.5 m and 1–2 m. These differences indicate the potential contribution of unmodeled tsunami sources, such as pyroclastic surge flows or explosive atmospheric pressure waves from secondary erupted, as noted by Self *et al*. (1984).

The combined modeling framework, incorporating both dense landslide and artificial wave scenarios, conceptually represents the spatial and temporal characteristics of the 1815 Tambora tsunami. Nonetheless, a multiphase numerical approach that integrates both mechanisms simultaneously would yield a more representative result, as demonstrated in the 1883 Krakatau case study (Maeno and Imamura, 2011), where complex source interactions better explained observed tsunami behavior.

4.2 Analysis of Tsunami Arrival Times

Historical records do not provide precise tsunami arrival times. However, the modeling results can still be compared qualitatively using the eruption chronology reconstructed by Self *et al*. (1984). The landslide scenario indicates that the first waves reach Sumenep approximately 115 minutes and Besuki about 125 minutes after the landslide occurs. These travel times align with the two-hour interval between the first major eruptive phase and the second major explosion, which began at 18:00 (GMT+8), with disturbances reported in East Java around 19:00 (GMT+7).

This relative consistency suggests that the tsunami observed in Sumenep and Besuki was most likely associated with the second eruptive phase rather than the earlier events. Although precise quantitative arrival times are not available, the qualitative agreement between the modeled propagation pattern and the historical chronology strengthens the interpretation that a dense-landslide mechanism can generate a wave-travel pattern similar to historical conditions.

It is important to note that this comparison is qualitative and not intended as a direct numerical match due to the limitations of historical documentation.

4.3 Evaluation of Tsunami-Generation Mechanisms

Overall, the findings indicate that the artificial-wave scenario tends to produce exaggerated outputs, both in terms of amplitude and unrealistically short arrival times. This suggests that the mechanism is not appropriate as a single explanation for the 1815 Tambora tsunami.

Conversely, the dense-landslide scenario provides more realistic results in near-source regions, both in terms of wave height and propagation patterns. However, in far-field regions, neither scenario is able to fully reproduce the historical wave heights. This implies that the Tambora tsunami was likely a multi-mechanism phenomenon involving more than one triggering process.

4.4 Scientific Implications

These results emphasize that volcanic tsunami modeling must consider combined triggering mechanisms, particularly in major eruptions with repeated eruptive phases such as Tambora. The integration of geological data, eruptive chronology, and numerical modeling is crucial for understanding wave-energy distribution and propagation characteristics.

This study provides initial evidence that dense pyroclastic deposit landslides represent the primary mechanism for explaining tsunami impacts in near-source regions, while far-field areas require additional model development to account for triggering mechanisms that were not captured in the present scenarios.

5. CONCLUSION

This study has evaluated and compared the accuracy of two tsunami-generation mechanisms for the 1815 Tambora eruption, namely the dense pyroclastic deposit landslide scenario and the artificial-wave scenario. The findings demonstrate that the dense-landslide scenario more accurately reproduces the historical characteristics of the tsunami in near-

source regions, particularly the wave heights observed at Tambora and Sanggar, which ranged around 5 to 6 meters and about 4 meters, respectively. In contrast, the artificial-wave scenario produces wave heights that are significantly higher than the historical accounts, indicating that it is not consistent with the documented near-field tsunami impacts.

In far-field regions such as Sumenep and Besuki, both scenarios tend to underestimate the historical wave heights of 1 to 2 meters. This suggests that additional processes, such as pyroclastic surges or atmospheric pressure waves, may have played a role in generating the tsunami in these more distant areas. While historical records do not provide precise arrival-time data, the qualitative comparison of modeled travel times with the eruption chronology suggests that the dense-landslide scenario aligns more closely with the known sequence of events.

Overall, this comparative assessment confirms that the dense-landslide mechanism provides the closest match to the historical tsunami observations in near-source regions, while the discrepancies in far-field areas highlight the need for future modeling efforts that incorporate additional triggering processes. In this way, the study has achieved its objective of determining which mechanism more accurately represents the historical characteristics of the 1815 Tambora tsunami.

6. ACKNOWLEDGEMENTS

This research is part of the projects titled “Korea-Indonesia Marine Technology Cooperation Research Center (20220512)” and “Establishment of the Integrated Ocean Fisheries Technology Training Center and the Enhancement of Capacity Building in Indonesia (PG54670)”, funded by the Korean Ministry of Oceans and Fisheries (MOF).

REFERENCES

Badan Informasi Geospasial. (2024): *BATNAS: Data Batimetri Nasional.* Retrieved December 23, 2024, from https://tanahair.indonesia.go.id/batnas/#/batnas

Badan Informasi Geospasial. (2024): *Indonesian Topographic Map (RBI).* Retrieved December 23, 2024, from https://tanahair.indonesia.go.id/batnas/#/batnas

Badan Koordinasi Nasional Penanganan Bencana. (2021): *Mengenal jenis bahaya letusan gunung api di Indonesia.* Retrieved May 6, 2024, from https://bnpb.go.id/berita/mengenal-jenis-bahaya-letusan-gunung-api-di-indonesia

GEBCO. (2024): *General Bathymetric Chart of the Oceans (GEBCO).* Retrieved December 23, 2024, from https://download.gebco.net/

Google Earth. (2024): *Satellite imagery data.* Retrieved December 23, 2024, from https://earth.google.com/web/

Grezio, A., Sandri, L., Gasparini, P., Argnani, A., Marzocchi, W., Gasparini, P., Selva, J. (2012): Probabilistic tsunami hazard assessment for the Messina Strait area (Sicily, Italy), *Natural Hazards*, 64(1), 329–358. https://doi.org/10.1007/s11069-012-0246-x

Harbitz, C.B., Løvholt, F., Pedersen, G., Masson, D.G. 2006: Mechanisms of tsunami generation by submarine landslides: a short review, *Norwegian Journal of Geology*, 86, 255-264.

International Tsunami Information Center. (2015): *Tsunami glossary.* Retrieved December 23, 2024, from https://www.tsunami.gov/?page=tsunamiFAQ

Kandlbauer, J., Sparks, R. S. J. (2014): New estimates of the 1815 Tambora eruption volume, *Journal of Volcanology and Geothermal Research*, 286, 93–100. https://doi.org/10.1016/j.jvolgeores.2014.08.020

Latief, H., Puspito, N. T., and Imamura, F. (2000). Tsunami catalog and zones in Indonesia, *Journal of Natural Disaster Science*, 22(1), 25–43. https://doi.org/10.2328/jnds.22.25

Maeno, F., and Imamura, F. (2011): Tsunami generation by a rapid entrance of pyroclastic flow into the sea during the 1883 Krakatau eruption, Indonesia, *Journal of Geophysical Research*, 116(B09205). https://doi.org/10.1029/2011JB008253

MAGMA Indonesia. (2021): *Volcano data for the period 416–2023.* Center for Volcanology and Geological Hazard Mitigation (PVMBG). Retrieved December 12, 2024, from https://magma.esdm.go.id/v1/edukasi/tipe-gunung-api-di-indonesia-a-b-dan-c

Paris, R. (2015): Source Mechanisms of Volcanic Tsunamis, *Philosophical Transactions of the Royal Society A: Mathematical, Physical and Engineering Sciences*, *373*(2053), p.20140380. https://doi.org/10.1098/rsta.2014.0380

Paris, R. (2025): *UNESCO-IOC webinar on monitoring and warning for tsunamis generated by volcanoes.* UNESCO Intergovernmental Oceanographic Commission. Retrieved April 16, 2025, from https://www.unesco.org

Pelinovsky, E., Zahibo, N., Dunkley, P., Edmonds, M., Herd, R., Talipova, T., Kozelkov, A., Nikolkina, I. (2004): Tsunami Generated by the Volcano Eruption on July 12-13, 2003 at Montserrat, Lesser Antilles, *Science of Tsunami Hazards*, 22, 44.

Pranantyo, I.R., Heidarzadeh, M., Cummins, P.R. (2021): Complex tsunami hazards in eastern Indonesia from seismic and non-seismic sources: Deterministic modelling based on historical and modern data, *Geoscience Letters*, 8 , 20. https://doi.org/10.1186/s40562-021-00190-y

Self, S., Rampino, M. R., Newton, M. S.,Wolff, J. A.

(1984): Volcanological study of the great Tambora eruption of 1815, *Geology*, 12(11), 659–663. https://doi.org/10.1130/0091-7613(1984)12<659:VSOTGT>2.0.CO;2

Sigurdsson, H., and Carey, S. (1989): Plinian and co-ignimbrite tephra fall from the 1815 eruption of Tambora volcano, *Bulletin of Volcanology*, 51, 243–270. https://doi.org/10.1007/BF01073515

Smithsonian Institution, National Museum of Natural History, Global Volcanism Program. (2024). *Tambora.* Retrieved December 12, 2024, from https://volcano.si.edu/volcano.cfm?vn=265050

Soloviev, S. L., and Go, C. N. (1984): *Catalogue of tsunamis on the western shore of the Pacific Ocean* (Canadian Translation of Fisheries and Aquatic Sciences, No. 5077). National Research Council of Canada, Canada Institute for Scientific and Technical Information. (Original work published 1974).

Stothers, R. B. (1984): The great Tambora eruption in 1815 and its aftermath, *Science*, 224(4654), 1191–1198. 10.1126/science.224.4654.1191

Suhendro, I., Toramaru, A., Miyamoto, T., Miyabuchi, Y., Yamamoto, T. (2021): Magma chamber stratification of the 1815 Tambora caldera-forming eruption, *Bulletin of Volcanology*, 83, 63. https://doi.org/10.1007/s00445-021-01484-x

The Conversation. (2019): *How Qantas and other airlines decide whether to fly near volcanoes.* Retrieved December 12, 2024, from https://theconversation.com/how-qantas-and-other-airlines-decide-whether-to-fly-near-volcanoes-117899

U.S. Geological Survey. (2024): *Earthquake search.* Retrieved December 25, 2024, from https://earthquake.usgs.gov/earthquakes/search/

Ulvrova, M., Paris, R., Nomikou, P., Kelfoun, K. (2014): Numerical simulations of tsunamis generated by underwater volcanic explosions at Karymskoye lake (Kamchatka, Russia) and Kolumbo volcano (Aegean Sea, Greece), *Natural Hazards and Earth System Sciences*, 14, 401-412.

Volcano Global Risk Identification and Analysis Project. (2023). *Tambora.* Retrieved December 12, 2024, from https://www2.bgs.ac.uk/vogripa/searchVOGRIPA.cfc?method=detaildanid=633

Watts, P. (1998). Wavemaker curves for tsunamis generated by underwater landslides, *Journal of Waterway, Port, Coastal, and Ocean Engineering*, 124(3), 127–137. https://doi.org/10.1061/(ASCE)0733-950X(1998)124:3(127)